2005 SCEC REPORT

Southern California Tectonic Deformation Modeling

Zheng-Kang Shen and **David D. Jackson**

Department of Earth and Space Sciences, UCLA

We have updated our results on southern California crustal deformation modeling and intermediate-to-long term earthquake forecast using geodetic information, and worked on two papers to document our findings. The results are the following.

1. Southern Calfornia Crustal Deformation Modeling.

We have updated our model of secular crustal deformation using the most recent Crustal Motion Map result. The SCEC Geodesy Working Group, in which Shen is a member, has been working on producing a new version of SCEC Crustal Motion Map, v4.0 (CMM4). So far a preliminary version of the product has been obtained (see Shen et al., SCEC Report: SCEC Crustal Motion Map, this year), which includes 892 GPS station velocities derived from continuous and survey-mode observations. As before a linked-fault-segment approach is used for the modeling. In this approach surface deformation is associated with dislocation along fault segments beneath the locking depth. Fault slip continuity is enforced by imposing finite constraints on slips along adjacent fault segments. Two end members emerge depending on the degree of constraints: strict constraints leads to a block-fault model, and loose constraints yields fault-segment-only model. Thus by optimally adjusting the degree of constraints, we are able to adopt the model to describe deformation not

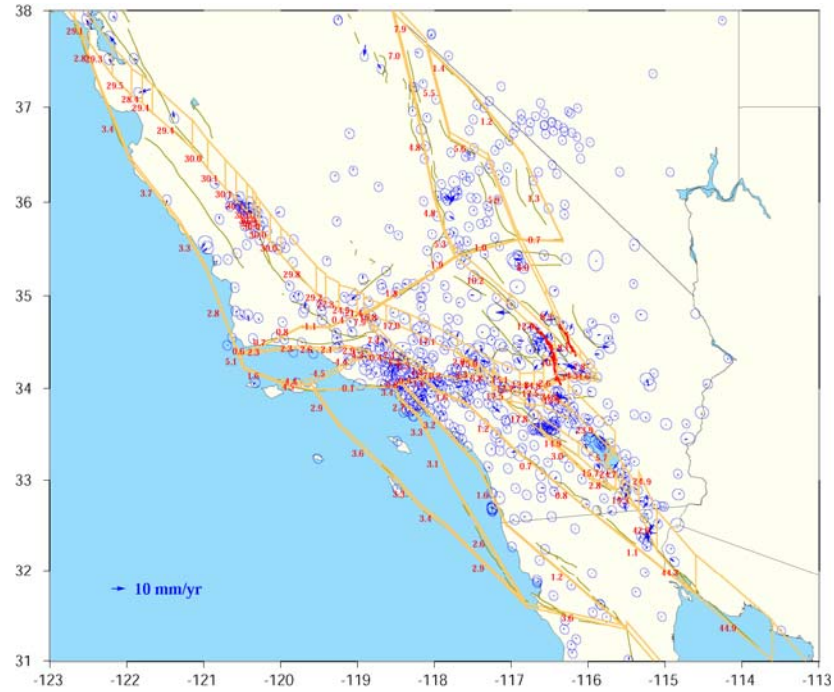

Figure 1. Post-Landers fault modeling result: strike slip component. Orange patches are modeled fault slip rates beneath locking depth, and their heights are proportional to the amplitudes of the slip rates. The number on each patch denotes its slip rate, right lateral positive. Red curves are the Landers and Hector Mine surface rupture traces. Blue arrows are postfit residuals of the velocity data. Error ellipses represent 95% confidence.

exactly “block-like”, yet still limiting the number of free parameters in the model. Fault geometry is defined using a simplified version of the SCEC Community Fault Model (CFM) and Community Block Model (CBM). The geodetic velocity field is used to invert for fault slip rates through the least-squares method, with the degree of constraints on fault continuation determined optimally through balancing a trade-off between the data postfit residual chi-squares and model resolution. We performed such inversions separately on data sets observed primarily before and after the 1992 Landers earthquake. For the latter solution the data observed following the 1999 Hector Mine earthquake and in its epicentral region are removed to keep the post-Hector Mine deformation field from entering the solution. In total 673 station velocities are used for the post-Landers inversion, which is 108 sites more than last year. The results are listed in Table 1 and the solutions for the strike slip and normal components are shown in Figures 1 and 2 respectively.

We then compared our new model result with the one we obtained last year. We found that major deformation patterns of the two models are pretty much the same. They include: (a) the slip rate changed along the SAF after the Landers earthquake, increasing along the sections of Coachella Valley from 20 to 24 mm/yr and Carrizo Plain from 27 to 30 mm/yr and decreasing along the Mojave section from 20 to 17 mm/yr; (b) the deformation rate across the Mojave Shear Zone changed significantly after the Landers earthquake, with the fault slip rate along the Blackwater fault increasing from 8 to 12 mm/yr; (c) the slip rate decreased along the San Jacinto fault by about 3 mm/yr after the quake, etc. We also report that among the fault normal components which are more reliably resolved, significant convergence is detected across the Santa Susana fault at ~4 mm/yr, Cucamonga fault at ~7 mm/yr, and Santa Cruz fault at ~7 mm/yr, respectively. About 5 mm/yr convergence is also detected across the Coachella section of the San Andreas fault (Table 1). Although the solution has not changed much, the uncertainties were reduced by as much as 50% by the substantial increase in the numbers of observations, particularly around the eastern California shear zone and in Mexico.

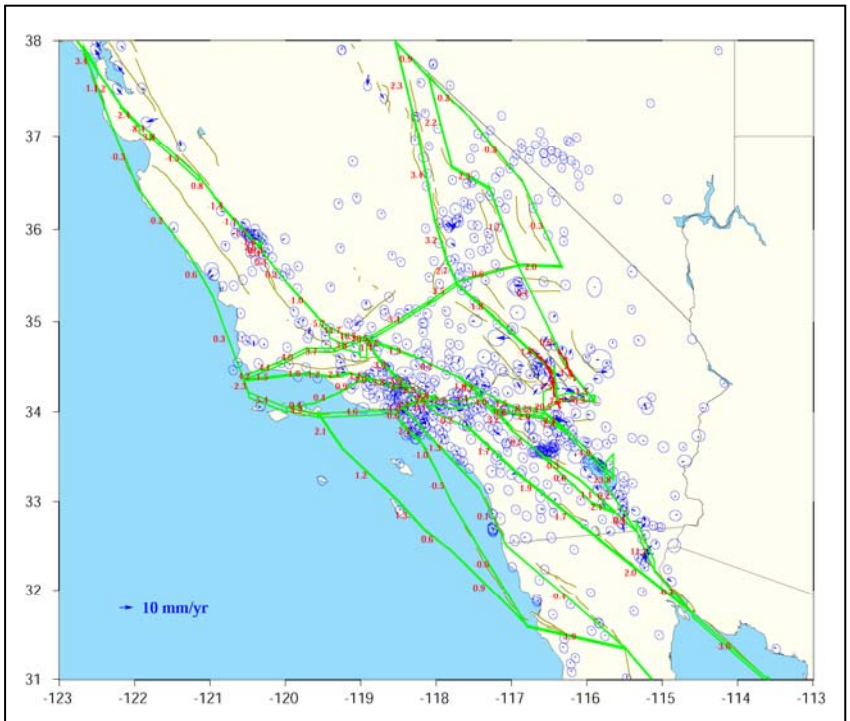

Figure 2. Post-Landers fault modeling result: normal component. Green patches are modeled fault slip rates beneath locking depth, and their heights are proportional to the amplitudes of the slip rates. The number on each patch denotes its slip rate, extension positive. The rest captions are the same as above.

We are now writing our findings into a paper, which we expect to finish by the end of this year. We are comparing our results with other studies, such as Meade and Hager (2005) and McCaffrey (2005), to assess the model differences and estimate the model validity and uncertainty.

Table 1. Fault slip rates

Fault	Vr	Vn	Rvr	Rvn	Fault	Vr	Vn	Rvr	Rvn
SAF-North	30	-1	0.17	0.22	Anacapa-Santa-Cruz	0	-5	0.45	0.33
SAF-Parkfield	30	0	0.39	0.29	Pinto-Mtn-West	-2	31	0.04	0.12
SAF-Carrizo	30	-1	0.16	0.16	Pinto-Mtn-East	-5	6	0.10	0.19
SAF-Tajon	24	-17	0.06	0.08	Oak-Ridge	-4	1	0.45	0.25
SAF-Mojave	17	0	0.50	0.51	Cucamonga	-3	-7	0.14	0.18
SAF-Cajon	13	-2	0.33	0.39	Sierra-Madre	5	-8	0.09	0.06
Banning	-13	2	0.27	0.15	San-Gabriel	6	-3	0.38	0.26
SAF-Coachella V	24	-5	0.53	0.35	Raymond	-2	3	0.09	0.05
Brawley	25	0	0.14	0.25	Santa-Monica-Malibu	-1	1	0.18	0.22
Imperial-Valley	25	0	0.25	0.14	Santa-Susana	6	-4	0.11	0.10
SAF-South	45	-3	0.21	0.05	San-Cayetano	2	-2	0.26	0.17
Mexico-South	8	0	0.46	0.19	Arroyo	2	-1	0.52	0.24
San-Clemente	3	1	0.63	0.35	Big-Pine	-1	4	0.41	0.42
New-Port-Inglewood	3	-1	0.54	0.35	San-Gregorio-Hosgri	3	0	0.58	0.49
Whittier	2	0	0.20	0.16	Garlock-West	-2	-3	0.45	0.54
Elsinore	1	2	0.97	0.69	Garlock-East	-1	1	0.43	0.63
SJF-North	18	-4	0.13	0.07	Owens-Valley	7	2	0.53	0.62
SJF-Central	18	2	0.34	0.17	Pisgah	8	1	0.39	0.33
SJF-South	19	2	0.77	0.15	Blackwater	12	-2	0.57	0.71
Superstition-Hill	3	-2	0.53	0.13	Hunter-Mtn-Param V	6	1	0.73	0.61
Palos-Verdes	3	-2	0.39	0.18	Death-Valley	1	0	0.48	0.33

Vr: Right slip; Vn: fault normal slip; R_{Vr}: right slip resolution; R_{Vn}: fault normal slip resolution

2. Intermediate-to-long Term Earthquake Forecast Using Geodetic Information.

We have constructed an earthquake likelihood model and use it to "forecast" earthquakes of M>5 in southern California for the next 5 years. The work has been written into a paper and submitted to the RELM special issue of Seismological Research Letters (Shen et al., 2005). Our model is based on the hypothesis that earthquake frequency and magnitude distribution are related to geodetic strain rate in two ways: a) seismicity rate is steady and proportional to the average horizontal maximum shear strain rate during the interseismic time period between large earthquakes; and b) earthquake magnitude distribution is spatially invariant except for an amplitude constant which is proportional to the maximum horizontal shear strain rate. The geodetic strain rate is derived by interpolating the velocity field from the Southern California Crustal Motion Map version 3.0 (CMM3, http://epicenter.usc.edu/cmm3). To "forecast" future earthquakes we screen out the stations whose average observation epochs occur before 1993.0.

In doing so we assure that the data were collected primarily after the 1992 Mw 7.3 Landers earthquake, the predominant source of recent transient deformation in southern California. GPS data collected in the epicentral area after the 1999 Mw 7.1 Hector Mine earthquake were removed from the CMM3 data set, thus the geodetic data set used to derive the strain rate field in this study could be regarded as the "post-Landers" deformation field, and was used to compare with the seismicity pattern after 1993. Interpolation of the station velocities is done through a series of regression steps using the method of Shen et al. (1996) and Jackson et al. (1997). In the process, a locally uniform strain rate field is assumed and the velocity data are reweighted by a Gaussian function exp $(-\Delta^2/\sigma^2)$, where Δ is the distance between a geodetic station and the spot being evaluated, and σ is an optimal smoothing distance determined through a trade-off between the formal uncertainty estimate of the strain rate and the total weight assigned to the data. The resulting maximum shear strain rate is shown in Figure 3.

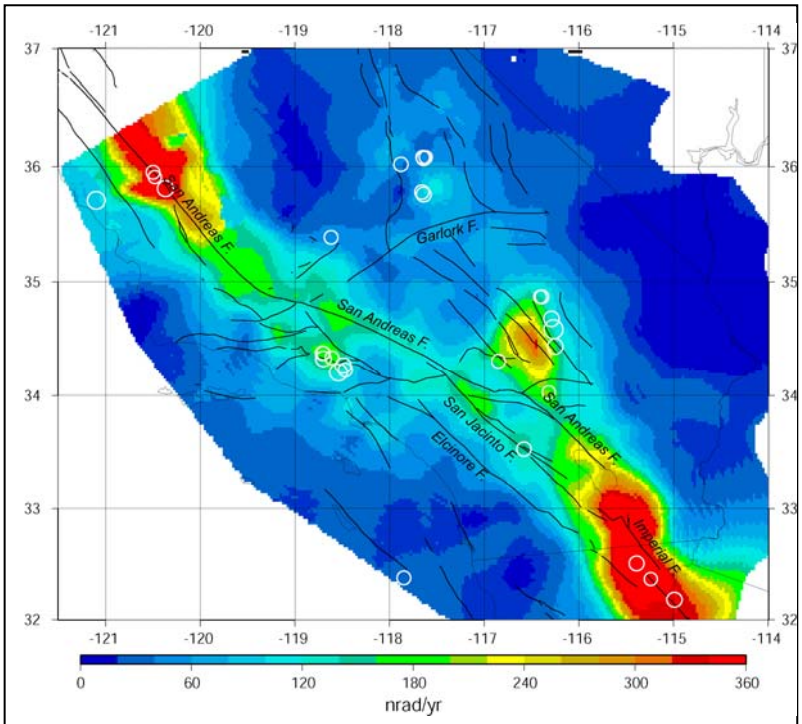

Figure 3. Maximum shear strain rate and earthquakes. Color contours show geodetically derived maximum shear strain rate at nano-radian/yr. Earthquakes of M≥5 occurred 1993-2005 are shown as white circles, with the size of the circles proportional to the magnitude.

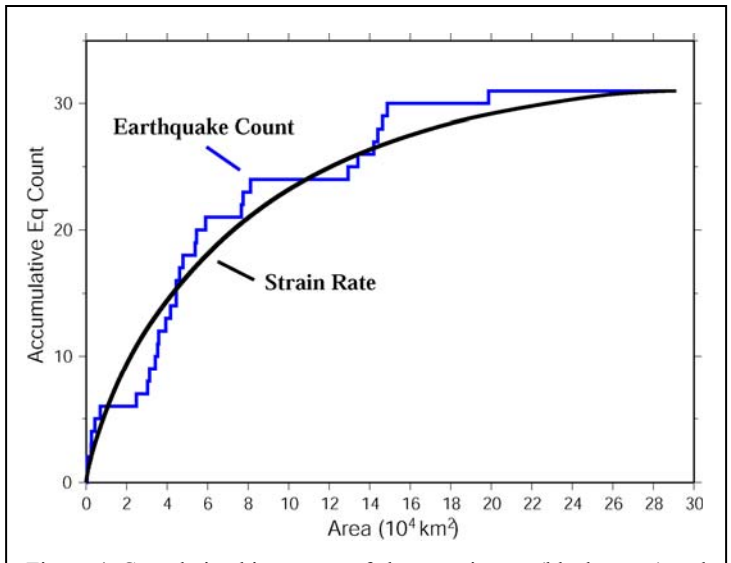

Figure 4. Cumulative histograms of shear strain rate (black curve) and earthquake count (blue curve). The shear strain rate with unit area is sorted in decreasing order, with the highest strain rate positioned to the left of the diagram.

We use the shear strain rate to "forecast" earthquakes from 1993.0-2005.5. This is considered a reasonable test because the coseismic and postseismic effects of the 1999 Hector Mine earthquake have been removed from the data, and the strain rate field should reflect the

steady state deformation over most of southern California. As revealed in Figure 4, ~75% of the earthquakes occurred within ~25% of the area with highest strain rate. Therefore our preliminary test of the method yields a cautiously promising result. Using this approach we have made a new forecast for the probability of the M ≥ 5 earthquakes in southern California for the next 5 years starting January 1, 2006 and the result will be given as an electronic supplement to the paper we submitted to Seismological Research Letters (Shen et al., 2005).

3. Correlation of Stress and Earthquakes

We computed the stress tensor in the upper crust of southern California as a function of time and compared observed seismicity with the estimated stress at the time of each earthquake (Kagan et al., 2005). We modeled crustal deformation using both updated geodetic data and geologically determined fault slip rates. We subdivided the crust into elastic blocks, delineated by faults which move freely as at a constant rate below a locking depth with a rate determined by the relative block motion. We computed normal and shear stresses on nodal planes for each earthquake in the catalog. We consider stress increments from previous earthquakes ("seismic stress") and aseismic tectonic stress, both separately and in combination. The locations and mechanisms of earthquakes are best correlated with the seismic shear stress. Including the cumulative coseismic effects from past earthquakes does not significantly improve the correlation. Correlations between normal stress and earthquakes are always very sensitive to the start date of the catalog, whether we exclude earthquakes very close to others and whether we evaluate stress at the hypocenter or throughout the rupture surface of an earthquake. Although the correlation of tectonic stress with earthquake triggering is robust, other results are unstable apparently because the catalog has so few earthquakes.

References to SCEC Publications:

SCEC Publication 822: Kagan, Y., D. D. Jackson, and Z. Liu, Stress and earthquakes in southern California, 1850-2004, J. Geophys. Res., 110, B05S14, doi:10.1029/2004JB003313, 2005.

SCEC Publication ???: Shen, Z.-K., D. D. Jackson, and Y. Kagan, Implications of Geodetic Strain Rate for Future Earthquakes, With a Five-Year Forecast of M5 Earthquakes in Southern California, submitted to *Seismol. Res. Lett*., 2005.

Other References

Bird, P, and Y. Kagan. Plate-tectonic analysis of shallow seismicity; apparent boundary width, beta, corner magnitude, coupled lithosphere thickness, and coupling in seven tectonic settings, *Bull. Seismol. Soc. Am.*, **94**, no.6, 2380-2399, 2004.

Jackson, D. D., Z.-K. Shen, D. Potter, X. Ge, L. Sung, Earthquakes and strain in southern California, *Science*, **277**, 1621-1622, 1997.

Kostrov, B. V., Seismic moment and energy of earthquakes, and seismic flow of rock, Izv. Acad. Sci. USSR. Phys. Solid Earth, 1, 23-40, 1974.

McCaffrey, R., Block kinematics of the Pacific-North America plate boundary in the southwestern United States from inversion of GPS, seismological, and geologic data, *J. Geophys. Res.*, **110**, B07401, doi:10.1029/2004JB003307, 2005.

Meade, B. J., and B. H. Hager, Block models of crustal motion in southern California constrained

by GPS measurements, *J. Geophys. Res.*, **110**, B03403, doi:10.1029/2004JB003209, 2005.

Shen, Z.-K., X. B. Ge, D. D. Jackson, D. Poter, M. Cline, and L. Sung, Northridge earthquake rupture models based on the global positioning system measurements, *Bull. Seismol. Soc. Am.*, **86**, 1B, S37-S48, 1996.